Fast late Pleistocene slip rate on the Leng Long Ling segment of the Haiyuan fault, Qinghai, China

C. Lasserre, Y. Gaudemer, P. Tapponnier, A. -S. Mériaux, J. van Der Woerd,
Yuan Daoyang, F. J. Ryerson, R. C. Finkel, M. W. Caffee

Fast late Pleistocene slip rate on the Leng Long Ling segment of the Haiyuan fault, Qinghai, China

C. Lasserre,[1,2] Y. Gaudemer,[1] P. Tapponnier,[1] A.-S. Mériaux,[1] J. Van der Woerd,[3] Yuan Daoyang,[4] F. J. Ryerson,[3] R. C. Finkel,[3] and M. W. Caffee[3]

[1] Fieldwork along the western Haiyuan fault, where it cuts young glacial landforms in the Leng Long Ling range (Qinghai, northeastern Tibet), yields new constraints on its long-term left-slip rate. Our mapping near 101.85°E, based on aerial photographs, 1/50,000 topographic maps, and SPOT images, shows glacial valley edges and lateral moraines offset ∼200 m by the fault. Quartz-rich cobbles were sampled on top of one moraine for in situ ^{10}Be and ^{26}Al cosmogenic nuclide dating. Among 12 dated samples, the 6 oldest show ages clustering at $10,300 \pm 339$ years. This age probably reflects the time of last reshaping of the moraine before the valley glacier withdrew south of the fault around the end of the Younger Dryas (≃11,000 years B.P.). Assuming that the 200 ± 40 m moraine offset started to be recorded after glacial retreat across the fault constrains the late Pleistocene slip rate on the Leng Long Ling segment of the Haiyuan fault to be 19 ± 5 mm/yr.   *INDEX TERMS:* 1035 Geochemistry: Geochronology; 8107 Tectonophysics: Continental neotectonics; 9320 Information Related to Geographic Region: Asia; *KEYWORDS:* Tibet, Haiyuan fault, neotectonics, fault slip rate, cosmogenic nuclide dating, glaciation

1. Introduction

[2] The convergence between India and Asia has produced one of the broadest zones of continental deformation on Earth (10^7 km^2), extending up to 3500 km north of the Himalayas [e.g., *Tapponnier and Molnar*, 1977; *Molnar and Tapponnier*, 1978]. The mechanisms of such large-scale deformation are debated [e.g., *Meyer et al.*, 1998, and references therein]. The relative importance of crustal thickening and strike-slip motion in absorbing convergence, as well as the proportion of strain accommodated by faults and localized shear zones are still controversial. Accurate determination of slip rates on the main faults in the collision zone is thus essential to help settling the argument.

[3] Together with the Altyn Tagh and Kunlun faults, the Haiyuan fault is one of the main left-lateral strike-slip faults of northeastern Tibet (Figure 1a), a particularly well-suited area to understand the mechanisms of deformation which led to the growth and rise of the Tibet plateau [*Meyer et al.*, 1998]. This ≃1000-km-long fault accommodates the east-

ward component of movement of Tibet relative to the Gobi-Ala Shan platform to the north [*Tapponnier and Molnar*, 1977; *Zhang et al.*, 1988a; 1988b]. The large 1920 Haiyuan ($M = 8.7$) and 1927 Gulang ($M = 8$–8.3) earthquakes occurred on and near the Haiyuan fault, respectively (Figure 1b) [*Deng et al.*, 1986; *Zhang et al.*, 1987; *Gu et al.*, 1989; *Gaudemer et al.*, 1995]. A ≃220-km-long seismic gap of great potential hazard has been identified along the western stretch of the fault [*Gaudemer et al.*, 1995] (Figure 1b). The average postglacial left slip rate on the western Haiyuan fault, east of its junction with the left-lateral Gulang fault and west of the Huang He, is now known to be greater than 1 cm/yr [*Lasserre et al.*, 1999]. Specifically, a rate of 12 ± 4 mm/yr, with a most likely minimum value of 11.6 ± 1.1 mm/yr, was obtained along the Maomao Shan segment of the fault (Figure 1b) from high-resolution geomorphological and geodetic data and ^{14}C dating. But along the Leng Long Ling segment of the fault, west of the junction between the Haiyuan and Gulang faults (Figure 1) and south of the eastern Qilian Shan range front, only loose estimates of the slip rate exist, ranging from 10 to 26 mm/yr [*Meyer*, 1991] and 10 to 20 mm/yr [*Gaudemer et al.*, 1995]. They derive from measurements of glacial feature offsets on SPOT images, and the assumption that the features postdate the Last Glacial Maximum (LGM) (18 ± 1 kyr B.P.) and predate the global warming at ≃12 ± 2 kyr B.P.

[4] To better assess the motion of NE Tibet relative to the Gobi, we carried out fieldwork northeast of Menyuan (Figures 1b and 2). Refining SPOT image analysis, we interpreted aerial photographs and 1/50,000 topographic

---

[1]Institut de Physique du Globe de Paris, CNRS UMR 7578, Paris, France.
[2]Now at Department of Earth and Space Sciences, University of California, Los Angeles, California, USA.
[3]Institut de Physique du Globe de Strasbourg, CNRS UMR 7516, Strasbourg, France.
[4]Seismological Institute of Lanzhou, China Seismological Bureau, Lanzhou, Gansu, China.
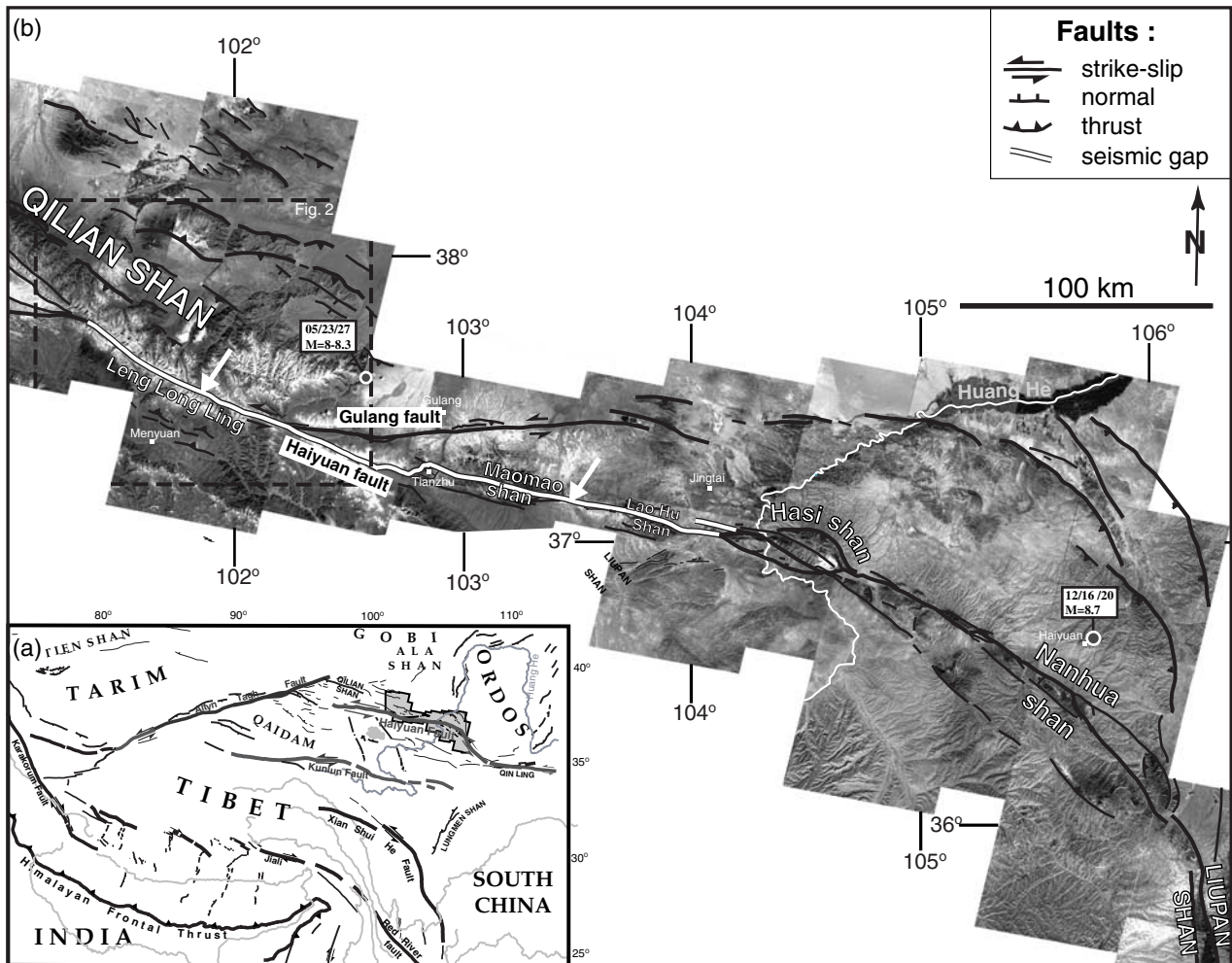
Figure 1. (a) Tectonic map of India-Asia collision zone. Haiyuan fault is outlined in gray. Shaded contour shows location of SPOT mosaic of Figure 1b. (b) Mosaic of SPOT images. Faults are from fieldwork and SPOT and Landsat images analysis. Tianzhu seismic gap [*Gaudemer et al.*, 1995] is outlined in white. Locations of 1920 and 1927 (dark gray dots), $M \geq 8$ earthquakes are from *Gaudemer et al.* [1995]. Arrows point to study sites where Haiyuan fault slip rate was determined from measurements and dating of geomorphic features offset by the fault (east, *Lasserre et al.* [1999]; west, this paper). Dashed box indicates location of Figure 2.

maps covering the study area and accurately measured geomorphic offsets. At one site, we sampled quartz-rich cobbles on the crest of a lateral moraine offset by the fault for cosmogenic nuclide dating (^{10}Be and ^{26}Al). The moraine offset and age yield a reliable value of the late Pleistocene slip rate along the Leng Long Ling segment of the Haiyuan fault.

2. Regional Geology and Landforms

[5] West of its junction with the Gulang fault, near 102.15°E, and east of 101.15°E, where it splays into several strands, the active Haiyuan fault displays a unique, sharp trace. It strikes N110°–115°E (Figure 2), 10–15° more southerly than the average strike of the western Haiyuan fault (Figure 1b). It follows the crest of the Leng Long Ling, a range composed mainly of exhumed Ordovician-Silurian rocks, whose highest, presently ice-capped summits culmi-

nate at 5254 m and 5024 m, north and south of the fault, respectively, about 30 km apart (Figure 2). In this region, the restraining bend of the fault [*Gaudemer et al.*, 1995] (Figures 1 and 2) leads to slip partitioning between the Leng Long Ling segment of the fault, which accommodates the strike-slip component of movement, and the Qilian Shan thrusts mostly to the north, which accommodate NNE shortening. The large northern thrusts are inferred to root on a southwest dipping décollement, which branches off the Haiyuan fault at a depth of ≃25 km [*Gaudemer et al.*, 1995]. They have raised the metamorphic basement (mainly Cambrian and Ordovician schists and igneous Mid-Paleozoic granodiorites and granites) to outcrop. Unconformed Devonian red beds and limestones, Carboniferous shales, Permian, Jurassic and Lower Cretaceous sandstones, and at places, Neogene sandstones covered by Quaternary conglomerates, are also exposed in WNW-ESE trending folds north of the Haiyuan fault. Most of the rivers draining this
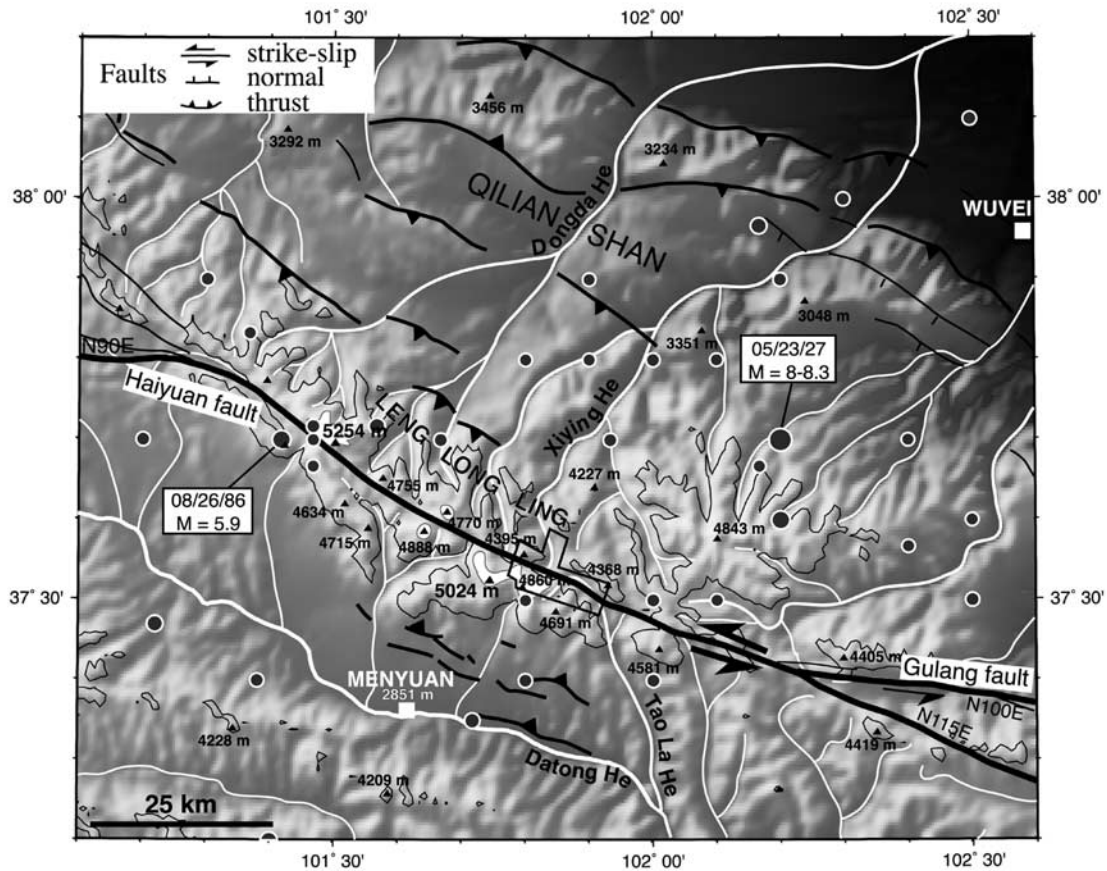
Figure 2. Seismotectonic map of Leng Long Ling area. Slip is partitioned principally between Haiyuan-Gulang strike-slip fault system and thrust system along Qilian Shan range front [*Gaudemer et al.*, 1995]. Note also active north dipping thrusts just north and east of Menyuan. Topography is from 30-arc sec Defense Mapping Agency DEM. Contour line at 4000 m is outlined. Main summit elevations are from 1/50,000 Gansu Geological Bureau or 1/500,000 TPC (Tactical Pilotage Chart) topographic maps. Ice-capped reliefs, in white, are from TPC maps. Main rivers are traced in white. Dark gray dots are $M \geq 4.5$ seismic events from *Gu et al.* [1989] (1920–1984), *Center for Analysis and Prediction* [1989] (1984–1988) and Seismological Institute of Lanzhou (1988–1998). Black irregular box indicates location of Figures 3 and 4.

uplifted area run off into the Tengger desert, north of Wuvei (Figure 2). Slices of Permian or Devonian sandstones are pinched along the fault [*Gansu Geological Bureau*, 1975a, 1975b; *Gaudemer et al.*, 1995]. South of the fault, Ordovician greenschists prevail. The southern flank of the Leng Long Ling is drained by rivers flowing into the Neogene Menyuan basin and the Datong He, a large tributary of the Huang He (Figure 2). North and east of Menyuan, active, north dipping, WNW-ESE striking thrusts and growing ramp anticlines are signaled by spearheaded, almond-shaped tongues of uplifted Neogene and Quaternary [e.g., *Meyer et al.*, 1998], limited to the south by the thrust traces (Figures 1b and 2). They probably also branch off the Haiyuan fault at depth.

[6] Quaternary glacial and periglacial processes have strongly contributed to shape the landforms of northeastern Tibet [*Derbyshire et al.*, 1991; *Lehmkuhl et al.*, 1998; *Van der Woerd et al.*, 2000, 2002], including the Leng Long Ling mountains. Glacial cirques, some still occupied by

glaciers, glacial valleys, glaciofluvial tills, and moraines can be mapped along the entire Leng Long Ling segment of the fault, on either side. Several glacial features cross the fault and are offset by it. Our field study specifically targeted one area near 101.85°E (Figures 1 and 2), already identified on SPOT images by *Meyer* [1991] and *Gaudemer et al.* [1995], where long-term offsets of glacial valley edges were particularly well preserved.

3. Site Field Study

3.1. Geomorphic Setting

[7] The ice-capped massif 25 km northeast of Menyuan is carved by several, 500-m to 2-km-wide glacial cirques, limited by fresh, steep and sharp bedrock crest lines. The massif culminates at 5024 m to the west, and 4860 m to the east (Figure 2). Our study was focused on the eastern part of the massif (Figures 3 and 4). On the north side, glacial valleys oriented N30°–45°E are partly occupied by present-
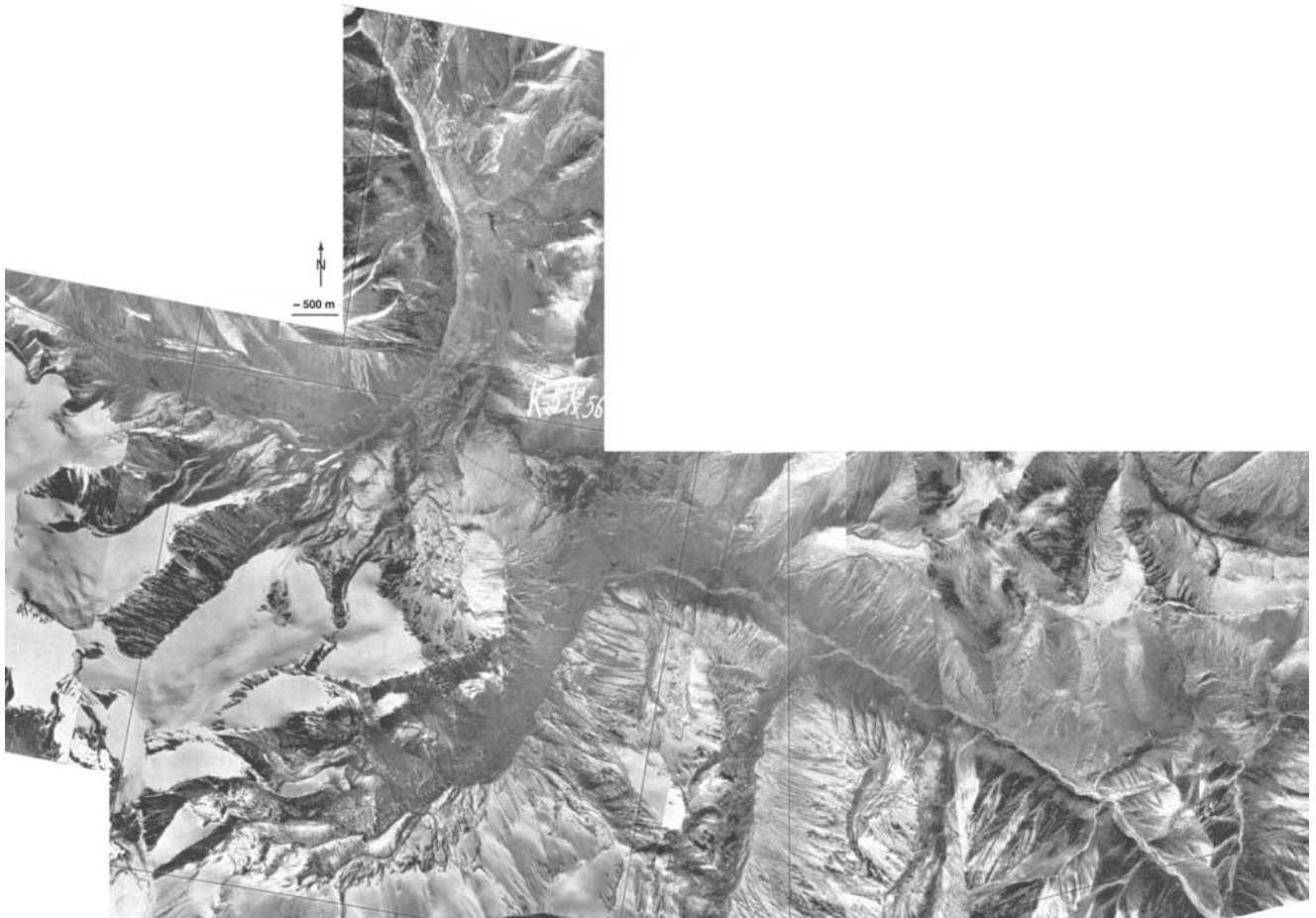
Figure 3. Mosaic of air photographs of Haiyuan fault, 25 km northeast of Menyuan (see Figure 2). Scale bar and orientation are only indicative, due to optical distorsion.

day glacial tongues, with lowest termini at elevations around 4150 m. The meltwaters of the glaciers feed outwash streams that merge principally into the Xiying He (Figures 2, 3, and 4). On the south side, glacier termini at elevations between ≃4200 and 4450 m give birth to streams that flow into the Datong He. One large river system, the Tao La He, flows northward before veering south to reach the Datong He, east of Menyuan (Figures 2, 3, and 4). Both the upper Xiying and Tao La He valleys show typical flat-floored, U-shaped sections, before narrowing abruptly to the north and southeast, respectively, implying incision by large glacial streams down to the narrows. Eastward, the maximum elevation decreases, with lowest summits ≃4400 m high, and ancient glacial cirques about 750 m wide are presently devoid of ice. West of the Tao La He valley narrow, the N115°E striking Haiyuan fault sharply bounds northern spurs of the ice-capped massif, cutting across the north flowing drainage network, the glacial valley edges, and moraine deposits (Figures 3 and 4), with dominantly strike slip movement. Both lateral edges of the valley of the easternmost tributary of the Xiying He show clear offsets (Figures 4, 5a, and 6). East of this valley, the fault also offsets the western edge of the Tao La He valley and the lateral edges of a former glacial valley downstream from a now abandoned glacial cirque (Figure 5b). Small-scale stream doglegs and free-faced scarps at the base of trian-

gular facets of Devonian sandstones mark the fault trace at several places (Figure 5a). Farther eastward, after crossing again the Tao La He, the fault locally veers to a N105°E direction, acquiring a component of north dipping normal throw. This is clear from both its geomorphic imprint and geological outcrops on incised sections (Figures 5c and 5d).

[8] On the basis of their relative heights, degree of degradation, surface characteristics and extent, four main units of glacial deposits can be distinguished in the Xiying and Tao La He valleys. The first unit, only ≃150–200 m below the present glacial termini, is made of dark-gray morainic till, completely free of soil and vegetation cover. We interpret it to mark the most recent advance of the glaciers during the Little Ice Age (330–80 years B.P. [*Liu et al.*, 1998]) (Figures 4 and 6). Small remnants of similar glacial deposits are also found in the upper parts of now empty cirques (Figure 5b). The second unit is composed of older, light gray, hummocky till, with sparse grass cover and collapse cracks. It fills the floors of the two glacial cirques in the frame of Figure 8, down to elevations of 3800–3850 m north of the fault (Figures 4, 6, 7, and 8). Two more conspicuous systems of morainic ridges, related to two yet more ancient, but more pronounced glacial advances, outline the edges of both the Xiying and Tao La He valleys. The lowest of the two systems (third unit), standing generally ≃150 m above the present bed of the glacial outwash,
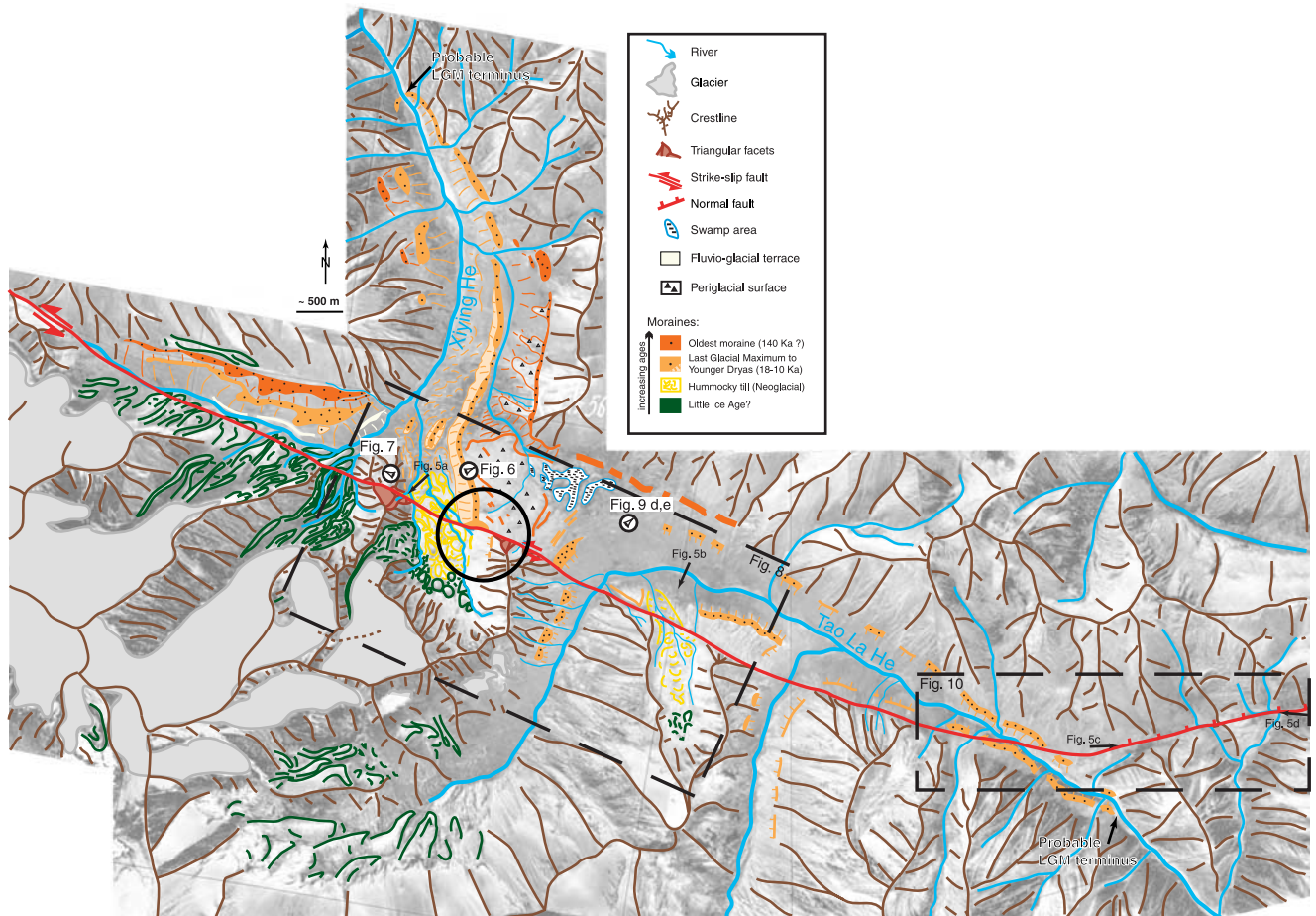
Figure 4. Geomorphic interpretation of glacial landscape of Figure 3 from field observations, air photos and satellite images analysis. Four principal moraine deposits are distinguished from their relative degrees of degradation, elevations, and maximum extent. Arrows point to locations of photos of Figure 5. Site where slip rate was determined is circled. Eye symbols point to view direction of photographs in Figures 6, 7, 9d, and 9e. Dashed boxes locate Figures 8 and 10.

is remarkably well preserved, particularly in the Xiying He valley (Figures 4 and 7). The shapes of the lateral and median morainic ridges, and even the closure of the most advanced frontal moraine across the outwash stream, look fresh and relatively young in the field as well as on SPOT images or aerial photographs. Despite smoothing by soil and grass, cobbles and boulders protrude out of the surface of all these moraines. The ring of boulders of the terminal frontal moraine transverse to the outwash corresponds to a knickpoint on the stream profile, right where the valley narrows, attesting to ice extension down to ≃3350 m, most likely at the time of the LGM (Figure 4). In the Tao La He valley, similarly clear lateral and terminal moraines can be mapped. The lowest frontal moraine, though less prominent, also stands where the valley narrows, at an elevation also close to 3350 m. The fourth and highest unit of till ridges, covered by thick loess and soil, stands 50 m above the third. It is fairly well preserved mostly in the Xiying He valley, particularly on the left bank, in the WNW-ESE oriented valley roughly parallel to the fault. There it extends all the way to the pass at 4124 m to the west (Figure 6). Although poorly preserved elsewhere, it can be mapped at the base of the ranges that bound the eastern and northern edge of the

Xiying and Tao La He valleys, respectively (Figure 4). A unique glacier, diverging downstream into two ice tongues, may thus have emplaced this most ancient unit of moraines.

[9] The freshest, longest, and most continuous morainic ridge observed lies along the right bank of the Xiying He, extending from the active fault trace, at ≃4000 m, down to the frontal moraine at ≃3350 m, over a distance of ≃6 km. It sags slightly for about 150 m north of the fault trace, then slopes with a gradient of 15−20% for 1.5 km, and more gently (≃10%, Figure 7) for the remaining distance down to its end. Clearly, this moraine once marked the eastern edge of a glacial valley, and formed as a lateral moraine of a glacier that flowed north from the cirque south of the fault. It now stands displaced from the edge of that cirque across the fault, as attested by the south facing facet visible in the field and on the maps and images (Figures 3, 4, 6, and 7). In the following sections, we focus on this particular site, where we measured the moraine offset and dated its emplacement using [10]Be and [26]Al cosmogenic nuclides.

3.2. Offsets Measurements

[10] On the north side of the fault, the intersection (piercing point) of the crest of the morainic ridge with the
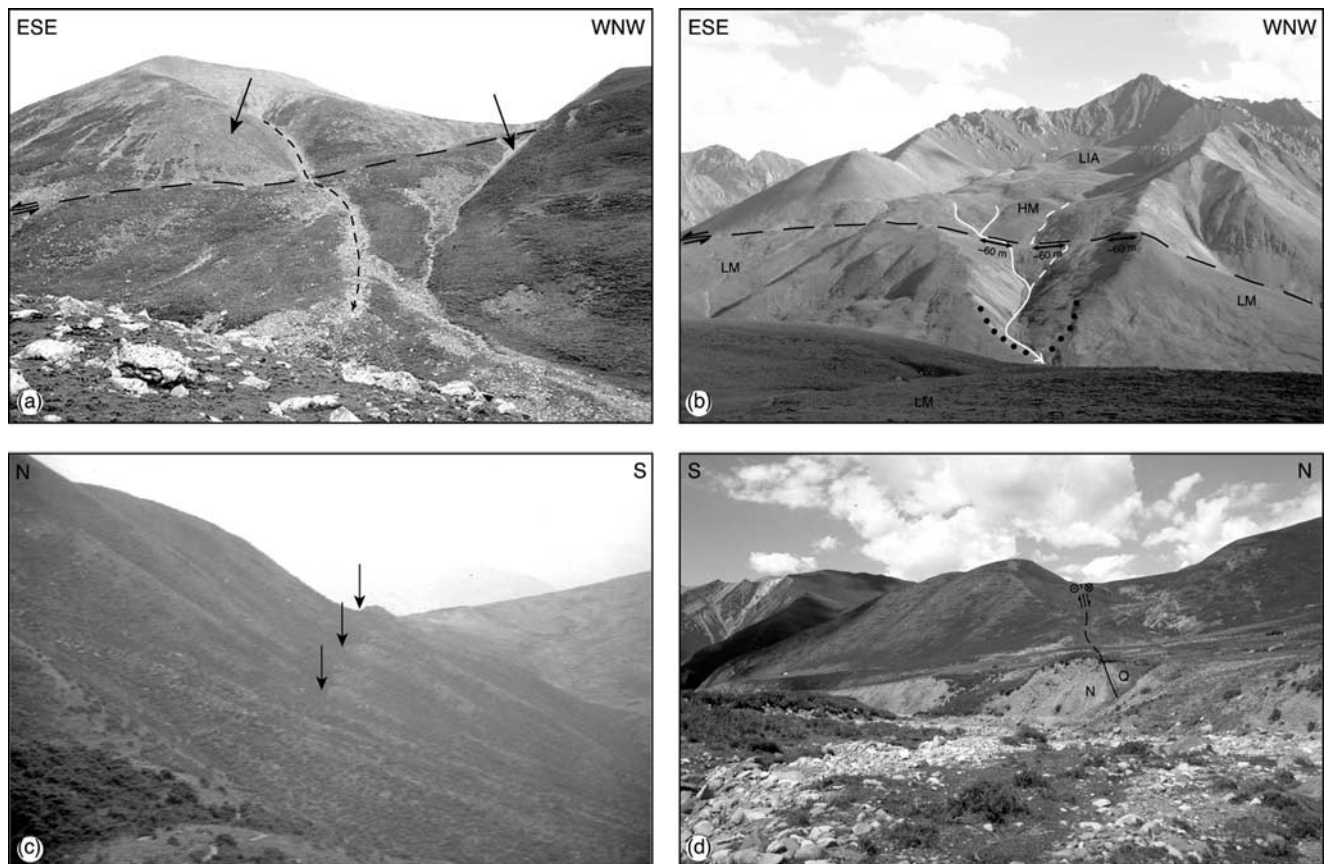
Figure 5. (a) SSW looking view of left edge of glacial cirque (circled in Figure 6), with long-term offset of ≃200 m. Fault scarp is outlined by faceted spurs in Devonian and Tertiary rocks on both sides of fault (arrows). Small gully in center of photo is offset ~10 m by fault. (b) SSW looking view of glacial cirque, presently free of ice, offset by the fault. Dark gray moraine deposits in upper part of cirque were probably emplaced during the Little Ice Age (LIA). Hummocky glacial tills (HM) filling cirque floor extend down north of fault, cutting older lateral moraine (LM) on right side of Tao La He trunk glacial valley (see also Figure 4). Dots mark terminus of hummocky till. Offsets of HM tills and small rills by fault is ≃60 m. (c) East looking view of north facing normal scarp, opposite to slope gradient. (d) West looking view of fault in eastern part of study area. Normal throw juxtaposes Neogene (N) with Quaternary (Q), in section on river bank.

fault trace is well defined (Figures 8a and 8b). On the south side of the fault, since no clear morainic ridge exists, the corresponding piercing point is the intersection between the fault and the steep valley side carved out of the bedrock by the glacier. Only slight traces of a bevel with possible coeval morainic deposits can be seen along that steep edge (Figure 7). We choose this piercing point to lie at the western tip of a triangular facet cut by the fault, considering that the surface of the glacier that deposited the moraine north of the fault must have been at least at the elevation of the base of that facet (Figures 8a, 8b, 9a, and 9b). Note that the probable remnants of the moraine aligned on the bevel south of the fault also intersect the fault at this point. Whether on the SPOT image, the air photographs or the 1/50,000 topographic map (Figures 8a–8c and 9c), we measure a distance of 200 m between the two piercing points, somewhat less than previously estimated from the SPOT image alone (250 m), without ground truth, by *Gaudemer et al.* [1995]. Considering that erosion possibly reshaped the moraine edge and given the uncertainty in

defining and mapping the triangular facet and the moraine edge, we consider an uncertainty of ±40 m (corresponding to ±2 pixels on the XS SPOT image and to less than ±1 mm on the topographic map) to be plausible.

[11] This offset value is not unique along the fault trace. It is found again on the western edge of the same glacial valley, which is offset by ≃200 m by the fault, as well as on the eastern edge of the valley just to the west (Figures 4, 6, and 8a–8c). On the west side of the Tao La He, before the river veers to follow the fault, the best preserved morainic ridge, which appears to be coeval with that in the Xiying He valley, is also offset 200 m (Figures 4, 8a–8c, 9d, and 9e). Where the Tao La He valley crosses the fault again farther east, it shows somewhat smaller but comparable sinistral offset (≃180 m), even though the small angle at which it intersects the fault trace makes that measurement less accurate (Figures 4 and 10). Matching the banks of the valley north and south of the fault also restores the continuity of two smaller streams channels incised in the mountains farther east.
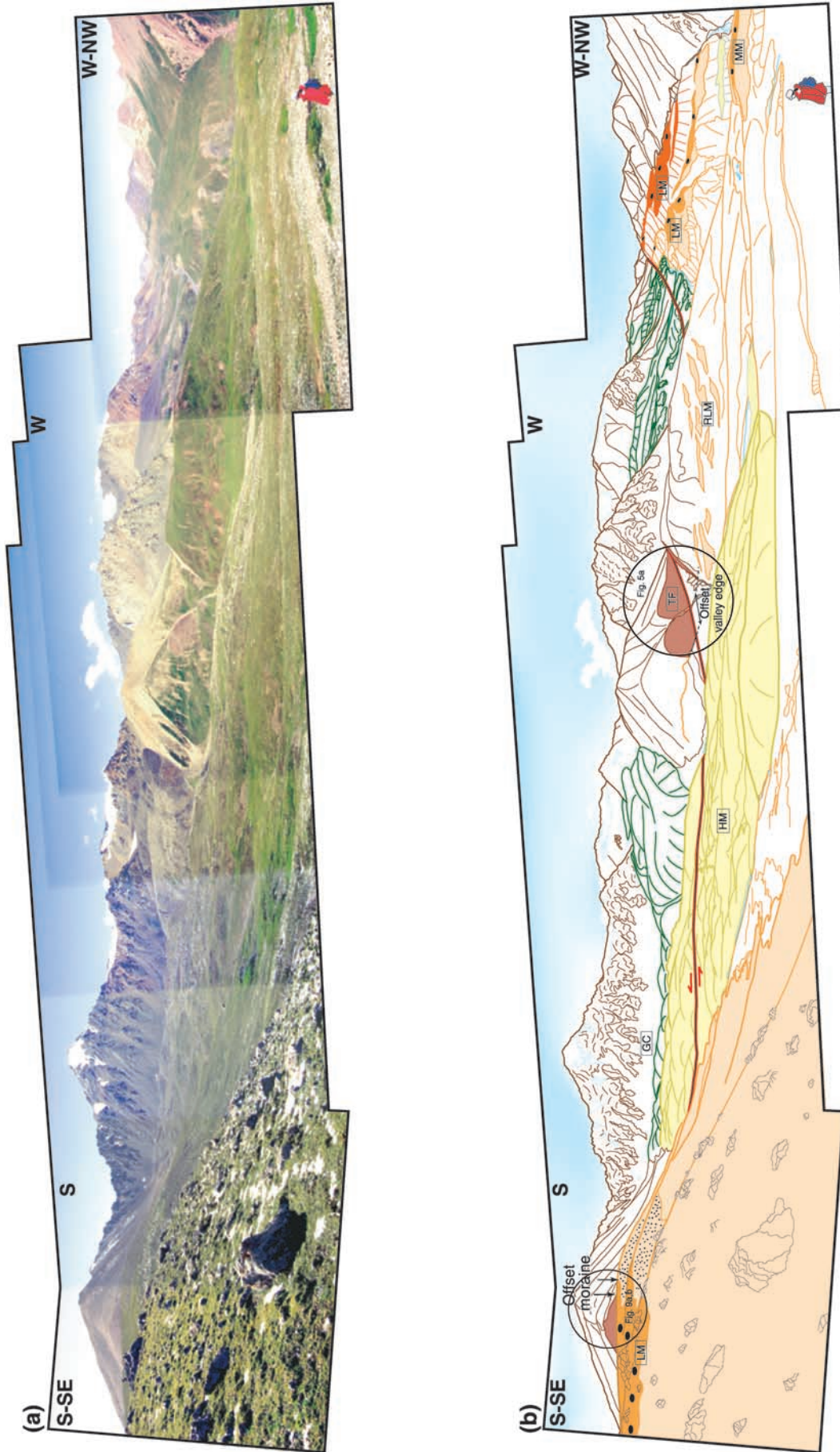
Figure 6. (a) SW looking view of glacial landscape at main study site (see Figure 4) and (b) corresponding geomorphic interpretation. Same color code as in Figure 4. GC, glacial cirque; HM, hummocky moraine; LM, lateral moraine; RLM, remnants of lateral moraine; MM, median moraine; TF, triangular facet. Circle on top left of photograph outlines offset moraine selected for cosmogenic dating and shows location of Figures 9a and 9b. Western edge of glacial cirque, circled in middle of photograph, is also offset.
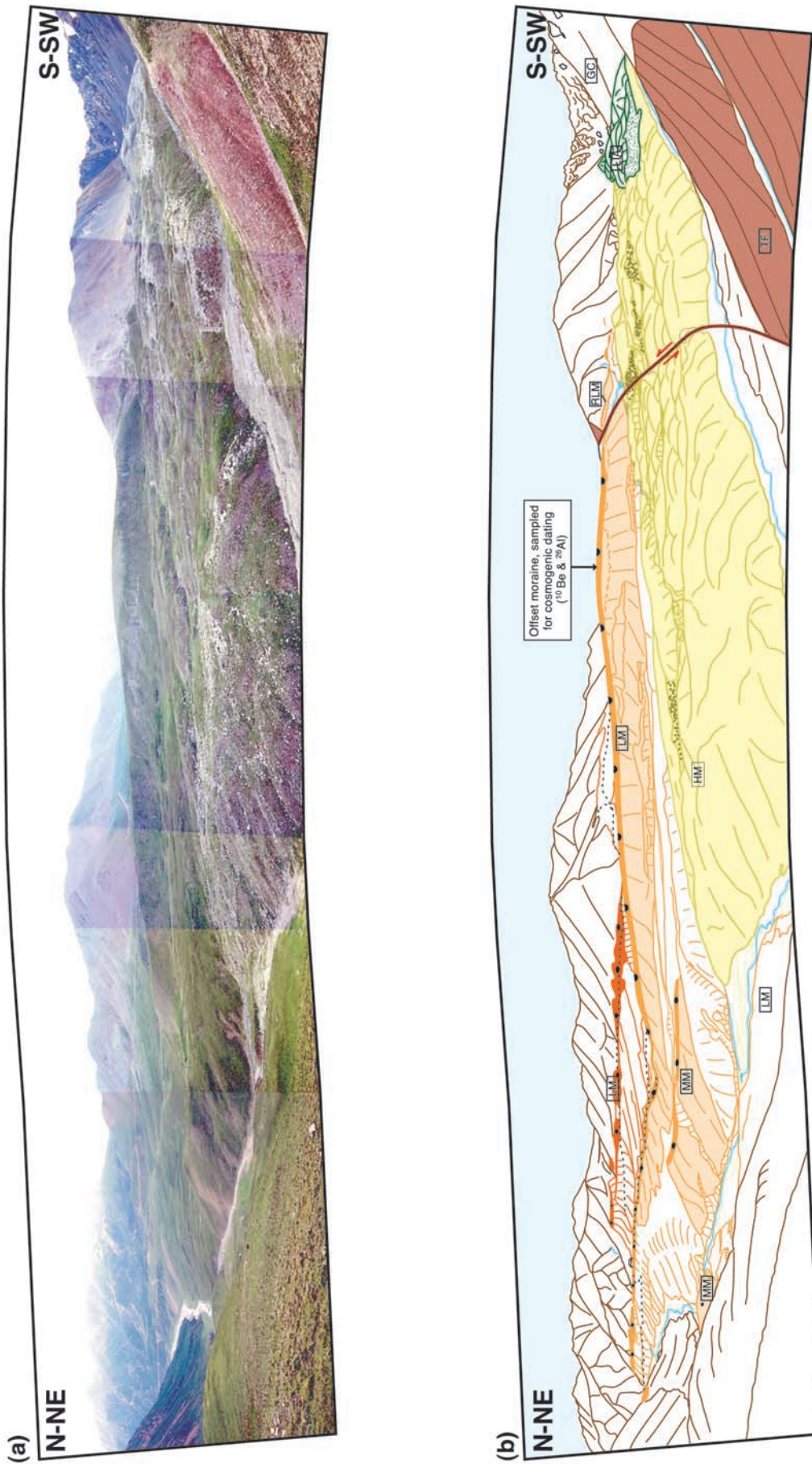
Figure 7. (a) SE looking view of study site (see Figure 4) and (b) corresponding geomorphic interpretation. Color code and symbols as in Figures 4 and 6. Best preserved morainic ridge, sampled for cosmogenic dating, in center of photo, can be traced all along the valley, down to its northern terminus. Arrow points to sagging part of moraine.
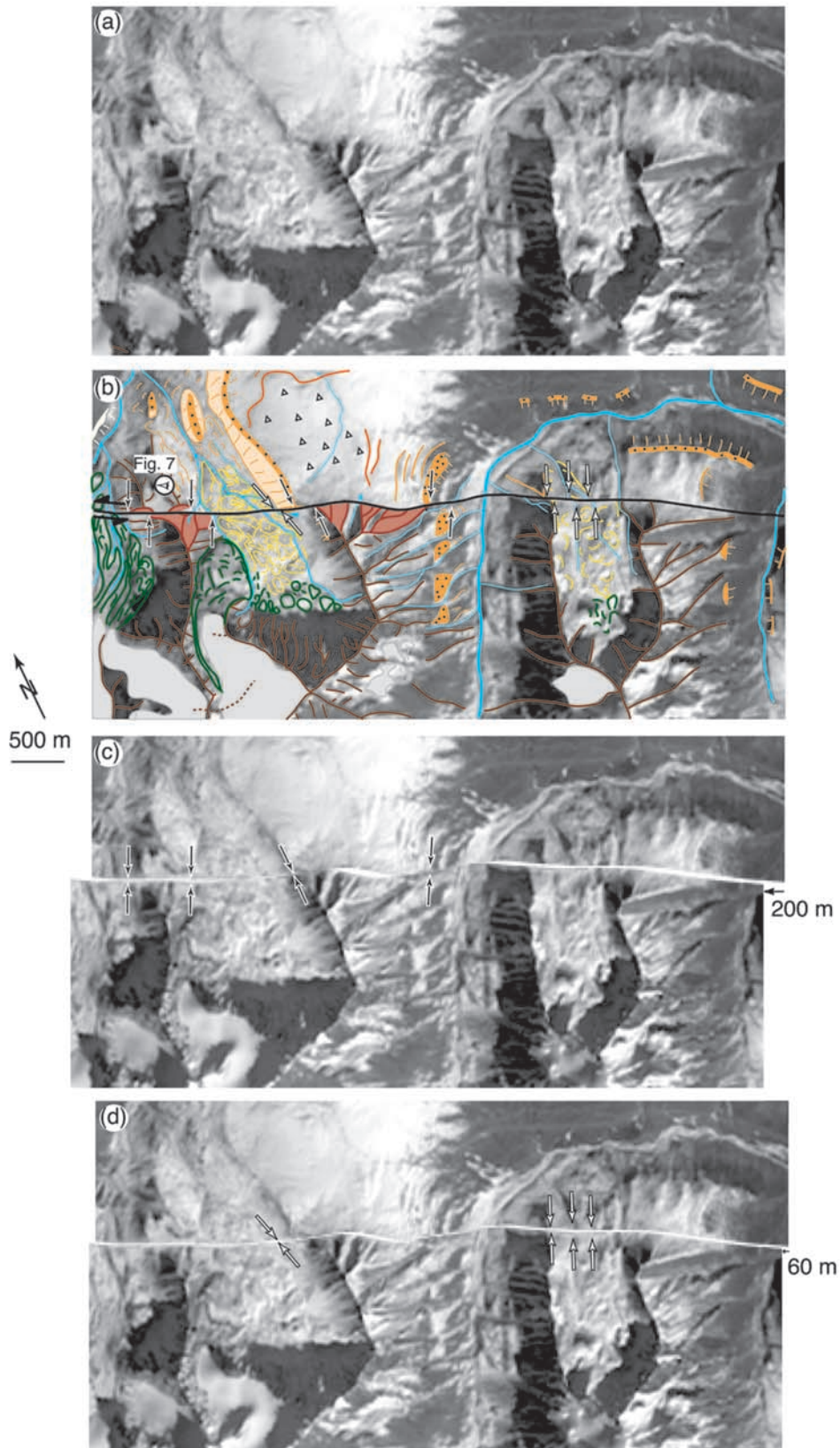
Figure 8. (a) Enlargement of XS SPOT image (KJ 252–275, 20 m pixel) of site (location on Figure 4) and (b) geomorphic interpretation. Color code as in previous figures. Black arrows outline glacial valley edges offset by ≃200 m. White arrows, hummocky till edges and rills offset by ≃60 m. Eye symbol points to view direction of photograph in Figure 7. (c) Best fit between blocks, restoring linear continuity of dated lateral moraine and glacial valley edges or (d) hummocky till edges.
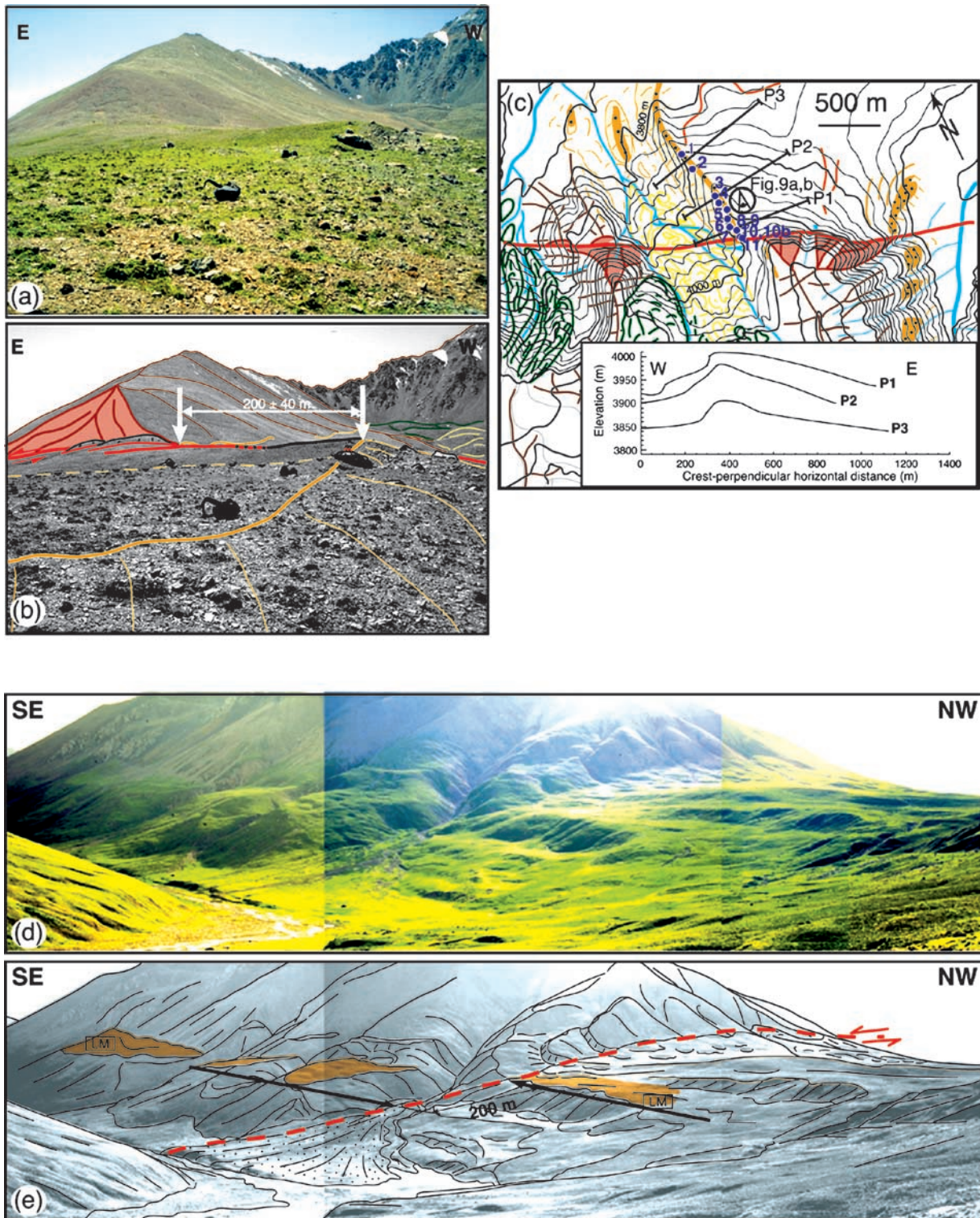
Figure 9. (a) and (b) South looking view of offset and dated moraine, showing selected piercing points for offset measurement (see discussion in text). Pressure ridges at base of triangular facet outline fault trace. (c) Sampling and geomorphic interpretation reported on topographic map (nominal scale 1/50,000). Numbered blue dots are quartz-rich samples collected for ^{10}Be and ^{26}Al dating. Lines transverse to moraine axis, north of fault trace, indicate location of topographic profiles P1 to P3, derived from the 1/50,000 map, in inset box. (d) and (e) SW looking view of morainic deposits bounding left side of upper Tao La He valley (see Figure 4 for orientation). Best preserved and largest level, correlated with dated offset moraine in Xiying He valley, is also offset by $\simeq$200 m. Note higher moraine levels with larger offsets NW of the fault.

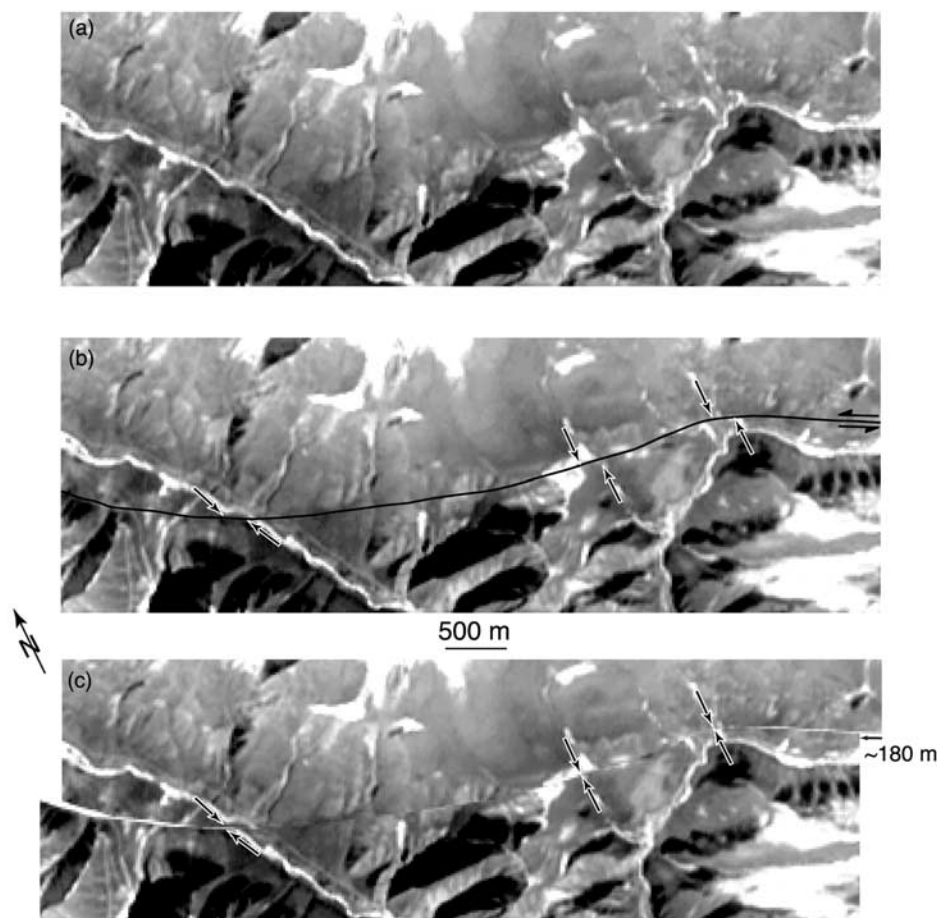**Figure 10.** (a) Enlargement of XS SPOT image (KJ 252–275, 20 m pixel) east of site area (location on Figure 4). (b) Arrows point to Tao La He and smaller stream channels dogleg offsets, whose linearity is restored by ≃180 m displacement along fault (c).

[12] Finally, the edges of the young hummocky tills filling the floor of the two glacial cirques in Figure 8 are offset by 60 ± 20 m by the fault (Figures 4, 8a, 8b, and 8d). This offset is particularly clear for the western edge of the eastern cirque (Figure 5b). Besides, the streams that flow down from this cirque, which incise and postdate the till, are offset by a similar amount. Such smaller offsets confirm that these hummocky glacial tills are younger than the ≃200 m offset lateral morainic ridges, in keeping with their fresh character and our geomorphic interpretation.

4. Slip Rate Determination by Cosmogenic Dating

4.1. Sampling and Calculation of Surface Exposure Ages

[13] To constrain the slip rate on the fault, we sampled the offset lateral moraine on the east side of the Xiying He valley for cosmogenic dating (Figure 8). The samples, located on a 1/50,000 topographic map in the field (Figure 9c and Table 1), were collected climbing the moraine crest from 3900 m up to its intersection with the fault, at ~4000 m. We estimate the uncertainty of their horizontal and vertical position to be ≃25 m and 20 m, respectively. The moraine boulders were mainly Devonian sandstones, with

quartz veins that we broke off with a hammer for sampling. The largest boulders observed on the moraine surface reached up to 5 m in diameter. We sampled the most common boulders (Figures 6 and 9a show the moraine surface character), with diameters smaller than 1 m (in most cases 20–30 cm). Each sample was ≃10 cm in diameter. We selected boulders embedded into the ground surface (protruding a few centimeters above the surface), as near from the morainic ridge crest as possible, with top surfaces as flat as possible, so that no correction for boulder geometry was needed, and no rotation or rolling of such boulders could be suspected.

[14] The exposure ages of 12 samples were determined using in situ [10]Be and [26]Al cosmogenic nuclide surface exposure dating. After grinding, quartz was separated from each sample using a chemical isolation method [Kohl and Nishiizumi, 1992]. Beryllium and aluminium were separated from the dissolved quartz by anion and cation exchange chromatography, precipitated as hydroxides and ignited to form oxides. The [10]Be/Be and [26]Al/Al ratios were determined by accelerator mass spectrometry (AMS) at the Lawrence Livermore National Laboratory (LLNL) AMS facility [Davis et al., 1990]. Measurements were normalized to ICN (ICN Biomedical, Inc., 1964) [10]Be and NBS [26]Al standards pre-

Table 1. Analytical Results of [10]Be and [26]Al Dating[a]

Sample	Elevation, m	Concentration, 10^5 atoms/g,[b]		Exposure Age, years,[c]		Ratio[d]
		[10]Be	[26]Al[d]	[10]Be	[26]Al[d]	
LLL1	3900	3.387 ± 0.234	18.002 ± 3.563	4664 ± 427	4147 ± 858	0.89
LLL2	3920	4.733 ± 0.234	24.884 ± 3.331	6454 ± 502	5678 ± 833	0.88
LLL3	3980	7.603 ± 0.386	40.513 ± 3.195	10061 ± 791	8979 ± 890	0.89
LLL4	3980	4.679 ± 0.233	25.841 ± 2.183	6186 ± 483	5718 ± 593	0.92
LLL5	3990	8.554 ± 0.469	47.243 ± 4.722	11264 ± 916	10425 ± 1215	0.93
LLL6	4000	1.893 ± 0.105	10.659 ± 9.616	2475 ± 202	2331 ± 253	0.94
LLL7	4000	2.830 ± 0.212	18.647 ± 1.397	3702 ± 355	4081 ± 392	1.10
LLL8	4000	6.832 ± 0.395	35.179 ± 2.132	8946 ± 746	7713 ± 658	0.86
LLL9	4000	7.798 ± 0.434	42.143 ± 2.493	10214 ± 836	9247 ± 779	0.91
LLL10[e]	4000	8.594 ± 0.429	43.772 ± 3.519	11260 ± 879	9606 ± 964	0.85
LLL10b[e]	4000	8.159 ± 0.420	56.273 ± 3.796	10688 ± 845	12366 ± 1116	1.16
LLL11	4000	2.698 ± 0.159	15.382 ± 1.382	3529 ± 297	3365 ± 364	0.95

[a] Samples, of ≃10 cm in diameter, were retrieved from boulders with diameters of 20–30 cm (in most cases) to 1 m. They were at latitude 37.5°E.
[b] Propagated analytical uncertainties include error on the blank, carrier, and counting statistics.
[c] Propagated uncertainties on the exposure ages include a 6% uncertainty on the production rate.
[d] Indicative values only because of [26]Al volatility during sample processing (see text).

pared by *Nishiizumi et al.* [1989]. Zero-erosion model ages were calculated using a sea level, high-latitude, [10]Be production rate of 5.2 atoms/g quartz/yr and a [26]Al production rate of 31.2 atoms/g quartz/yr. These production rates are based on measurements on glacial surfaces in the Sierra Nevada by *Nishiizumi et al.* [1989]. They were recalculated using the revised 13,000-year glacial retreat ages reported by *Clark et al.* [1995] and rescaled for latitude and elevation using the coefficients of *Lal* [1991], as described by *Owen et al.* [2002]. The ages we provide include an uncertainty of 6% on the production rates [*Stone*, 2000]. Shielding by the surrounding topography, which was small as estimated from 1/50,000 topographic maps (Figures 6, 7, and 9c), was neglected. The results are listed in Table 1.

4.2. Interpretation of Ages and Slip Rate Determination

[15] The [26]Al/[10]Be exposure age ratio is below the typical value of 1 (Table 1). During this study and other investigations, we have determined that this apparent discordance is an analytical artifact due to Aluminium volatility during sample processing. This has been confirmed by experiments using standard solutions. We will thus base all subsequent discussions on [10]Be exposure ages only. However, given the current uncertainties in the [26]Al data, the observed [26]Al/[10]Be exposure age ratio is indistinguishable from 1, confirming that our samples have had a simple exposure history.

[16] Six samples over a distance of ≃350 m along the crest yield ages of 9000–11,000 years (LLL3, 5, 8, 9, 10, and 10b). The other six (LLL1, 2, 4, 6, 7, and 11) have ages younger than ≃6500 years (Table 1 and Figure 11b). None of the ages obtained are older than ≃12,000 years, and the ages of the oldest samples cluster around 10,300 ± 339 years (weighted mean of the six oldest ages). Considering moraine weathering, boulder erosion or snow shielding within reasonable bounds would not change significantly our relatively young model ages (see *Gosse and Phillips* [2001] for quantitative estimates of these effects). We interpret the ≃10,300 year age to reflect the time of last reshaping of the lateral moraine by the glacier, shortly

before it withdrew across the fault at the end of the Younger Dryas (≃11,000 years B.P.), before the onset of the warmer Holocene period (10,000 years B.P.). Although the limit of ice extension during the short Younger Dryas cold spell remains poorly known, there is little doubt that the particularly fresh terminal moraine observed downstream at ≃3350 m in the Xiying He valley marks the maximum extension of the Xiying He valley glacier at the time of the Last Glacial Maximum, the last and greatest regionally documented glacial event (LGM, 18 ± 1 kyr in northern Tibet [*Thompson et al.*, 1997]).

[17] Regarding the other samples, two of the youngest samples LLL6 and LLL7 (≃2500 and 3700 years, respectively, Table 1) are located near each other, close to the steep sagging part of the moraine, which shows significant degradation (Figure 7; profile P2 in Figures 9c and 11b). We infer that these two samples, close to the morainic edge, were only recently exhumed and exposed to cosmic rays, as the moraine was reshaped by lateral erosion. For the two samples collected at the lowest elevations (LLL1 and LLL2), their position on a particularly steep part of the morainic ridge (Figures 9c and 11b) may similarly account for their young ages (≃4700 and 6500 years, respectively).

[18] The slip rate depends on the age attributed to the 200 ± 40 m offset of the moraine. Since the Xiying He valley glacier likely reached its maximum development, hence maximum incision and transport power, at the time of the LGM, a lower bound on the slip rate (11 ± 3 mm/yr) is obtained assuming that all the offset accrued since 18 ± 1 kyr ago. An alternative, more likely scenario, however, is one in which the offset is considered to have accumulated since the glacier withdrew definitively upstream from the fault. When estimating the slip rate on a fault using strath terrace risers as offset markers, the offset age is generally taken to be that of abandonment of the lower terrace [e.g., *Weldon and Sieh*, 1985; *Gaudemer et al.*, 1995; *Van der Woerd et al.*, 1998; *Lasserre et al.*, 1999]. This is because a terrace riser is rejuvenated by lateral cutting as long as the river flows along its base. It thus starts recording cumulative fault slip only after the terrace at its base has been completely abandoned by the river. Following a similar line
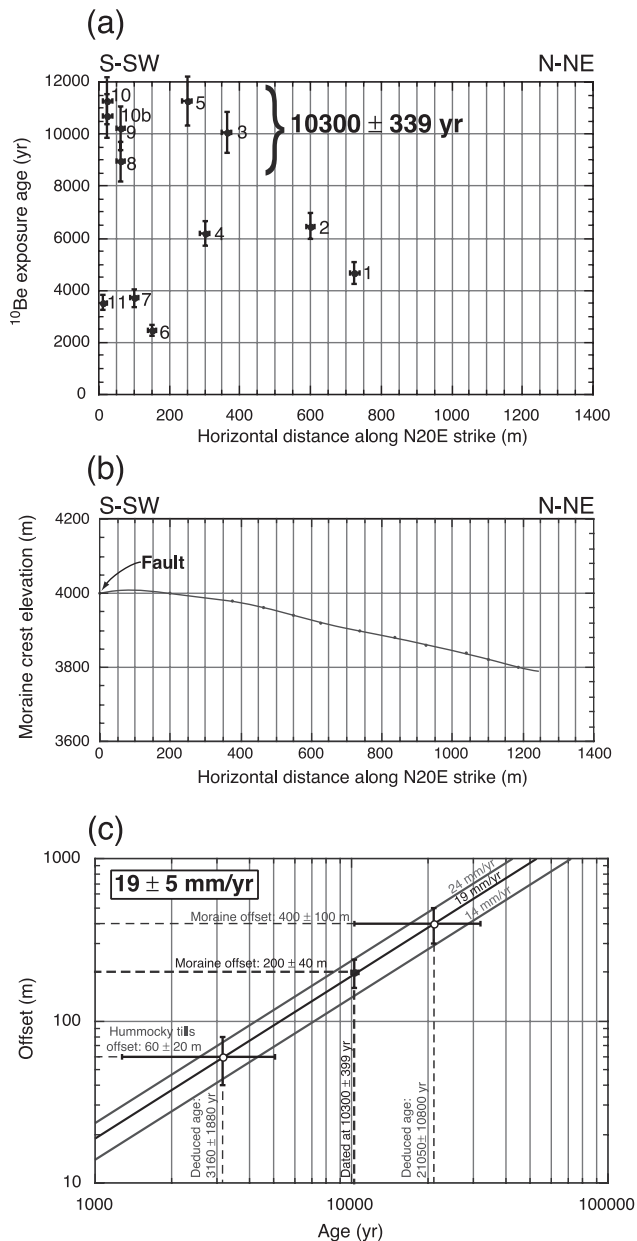
Figure 11. (a) Plot of sample ages in relative position along moraine crest and (b) topographic profile of moraine crest projected on N20°E striking vertical plane, from fault northward. (c) Late Pleistocene left slip rate deduced from cosmogenic dating of lateral moraine at study site. Hummocky till edges and rill offsets (≃60 m) age would be 3160 ± 1880 years.

of reasoning, we assume that, as long as a glacier crosses a fault, its abrasion power is enough to keep lateral moraines straight across the fault, smoothing or cancelling altogether slowly growing dogleg offsets. This scenario seems particularly plausible at our study site. The fault hugs the mountain front, at the limit between the glacially carved bedrock cirques and the periglacial piedmont, where unconsolidated moraines were deposited. Lateral erosion and transport where the glaciers cross the fault must therefore have been important. Consequently, sharp, dogleg moraine offsets at the fault, particularly on the right side of the

valleys, should not have begun to accrue prior to complete glacier retreat across the fault. The age of the 200 ± 40 m lateral moraine offset is thus likely to be that of ultimate glacier withdrawal across the fault, shortly after it deposited the oldest boulders found on the lateral moraine, at 10300 ± 339 years, a time that coincides with the end of the last climatic cold spell. This yields a slip rate along the fault of 19 ± 5 mm/yr (Figure 11c).

[19] The total offset of the moraine accumulated since the LGM may be preserved farther from the fault trace. The large-scale sigmoidal shape of this lateral moraine (Figures 3 and 4), which bends northeastward about 900 m north of the fault, may reflect such a longer-term cumulative offset. This offset can be loosely estimated to be on order of 400 ± 100 m. Such a bend, on the other hand, might result, at least in part, from other factors causing a sinuous course of the Xiying He glacier. On the west side of the adjacent Tao La He valley, besides the ≃200 m offset of the most prominent western lateral moraine, which we also infer to be coeval with the end of the Younger Dryas, a cumulative offset of other, higher morainic ridges, also on order of 400 m, seems to have been preserved (Figures 3, 4, 8a–8c, 9d, and 9e). Such higher moraines, probably preserved here because they are located on the left edge of the formerly glaciated valley, where it veered sharply southeastward, are likely to have been emplaced during the LGM. In either valley, offsets on order of 400 m in about 20 kyr would be compatible with a ≃20 mm/yr slip rate (Figure 11c). Finally, the observation that the Tao La He and two other river channels east of it show sinistral offsets on order of 180 m (Figure 10), is consistent with the inference that these rivers incised their channels more deeply at the beginning of the early Holocene pluvial, ≃9000–10,000 years ago, and with a slip rate on order of 20 mm/yr. All these different geomorphic observations are consistent with the offset and timing scenario we propose, making the corresponding 19 ± 5 mm/yr slip rate deduced from it quite likely.

[20] Given this slip rate and assuming it has remained uniform since about 20 kyr, the hummocky till deposits offset 60 ± 20 m by the fault (Figures 5b and 8) would have been abandoned by the retreating glaciers around 3160 ± 1880 years (Figure 11c). Thus, despite the large uncertainty, such tills can be plausibly related to one of the neoglacial climate fluctuations that have marked the last 3600 kyr [*Shi et al.*, 1986]. Incision of the small rills that are offset by similar amounts (Figure 5b) would also be related to an immediately subsequent pluvial. The age of the highest moraine level visible in the regional landscape, which remains distant from the fault (Figure 4), is unknown. But the corresponding deposits might plausibly have been emplaced either during the Riss Glacial Maximum (stage 6, ≃140 kyr) or at some early stage of the Würm period (between 110 and 60 kyr), prior to the LGM. It is likely that the geometry of the glacial confluence network at the time was quite different from that which appears to have characterized the last 20 kyr.

5. Summary and Discussion

[21] The long-term, ≃200 m offset, by the Leng Long Ling segment of the Haiyuan fault of the Xiying He lateral moraine, whose last reshaping appears to have occurred

around 10,300 years ago, constrains the late Pleistocene sinistral slip rate on this segment of the fault to be 19 ± 5 mm/yr. A conservative, unlikely, lower bound would be 11 ± 3 mm/yr. The ≃19 mm/yr rate is consistent with previous estimates by *Meyer* [1991] and *Gaudemer et al.* [1995], which ranged between 10 and 26 mm/yr. They had identified moraine or glacial valley edge offsets, on order of 200 to 270 m, at several sites in the Leng Long Ling, though on SPOT images only. In the absence of absolute chronological data, they inferred the offsets to have accrued in the period since the LGM or the onset of the Holocene. Our dating, using ^{10}Be and ^{26}Al cosmogenic nuclides, of the offset Xiying He moraine at 10,300 ± 339 years thus confirms and refines their early, first-order estimates. Much of the glacial morphology studied in the field indeed appears to reflect the imprint of the LGM and of subsequent climatic events. The maximum recent extent of valley glaciers, down to ≃3350 m, most likely took place around the LGM (≃20 kyr ago). The Xiying He lateral moraine we dated was most likely last reshaped and abandoned at the end of the Younger Dryas. The 19 ± 5 mm/yr slip rate we obtain in our study is fully consistent with the slip rate of 12 ± 4 mm/yr measured on the Maomao Shan segment of the fault, toward the east, past the splay of the Gulang fault [*Lasserre et al.*, 1999]. It is also in keeping with a westward increase of slip rate as the two faults merge and with the slip contribution of the Gulang fault previously estimated to be 4.3 ± 2.1 mm/yr [*Gaudemer et al.*, 1995] (Figure 1).

[22] On the other hand, our results, which imply fairly fast eastward shear of NE Tibet relative to the Gobi, 70% faster than between central and NE Tibet along the Kunlun fault [*Van der Woerd et al.*, 1998, 2000, 2002], are markedly different from indirect inferences derived from regional GPS campaigns [*Chen et al.*, 2000]. This may reflect either the still small number of measurement epochs and stations used in such studies, or more fundamental differences in short and long-term crustal fault mechanics. A long-term sinistral slip-component as high as ≃2 cm/yr between NE Tibet and the Gobi east of 100°E has important implications for our understanding of the deformation of central Asia [*Peltzer and Saucier*, 1996]. It would confirm that bookshelf faulting is an incorrect description of current strain on the east side of Tibet [*Avouac and Tapponnier*, 1993]. It would also be in keeping with a sinistral slip rate faster than ≃2 cm/yr on the eastern Altyn Tagh fault [*Meyer et al.*, 1998; *Mériaux et al.*, 1998], rather than with the much smaller values inferred from a two epoch GPS campaign study at ≃91°E [*Bendick et al.*, 2000]. Clearly, accurate dating of geomorphic offsets is a key to quantitative assessment of long-term, average slip rates on major active faults. The growing number of studies efficiently combining AMS ^{10}Be and ^{26}Al dating with quantitative neotectonics fieldwork [*Mériaux et al.*, 1997, 1998; *Mériaux*, 2002; *Van der Woerd et al.*, 1998, 2000, 2002] is yielding a fast increase in reliable constraints on the late Pleistocene-Holocene slip rates on a few of these faults (Kunlun, Altyn Tagh, Haiyuan). This effort should be sustained.

[23] One important byproduct of such work, including that presented here in the Leng Long Ling ranges of Qinghai province, is a better, large-scale understanding of Quaternary glaciations and other climatic events in northeastern Tibet, many aspects of which are still hotly debated [e.g., *Lehmkuhl et al. 1998*]. More such work is thus also needed to constrain and improve models of both crustal deformation and climate change, and of possible coupling between the two [e.g., *Ramstein et al.*, 1997; *Fluteau et al.*, 1999].

References

Avouac, J.-P., and P. Tapponnier, Kinematic model of active deformation in central Asia, *Geophys. Res. Lett.*, 20, 895–898, 1993.

Bendick, R., R. Bilham, J. Freymuller, K. Larson, and G. Yin, Geodetic evidence for a low slip rate in the Altyn Tagh fault system, *Nature*, 404, 69–72, 2000.

Center for Analysis and Prediction, China Seismological Bureau, *Earthquake Catalogue in West China*, Science Press, Beijing, 1989.

Chen, Z., B. Burchfiel, Y. Liu, R. King, L. Royden, W. Tang, E. Wang, J. Zhao, and X. Zhang, Global Positionning System measurements from eastern Tibet and their implications for India/Eurasia intercontinental deformation, *J. Geophys. Res.*, 105, 16,215–16,227, 2000.

Clark, D. H., P. R. Bierman, and P. Larsen, Improving in situ cosmogenic chronometers, *Quat. Res.*, 44, 367–377, 1995.

Davis, J. C., et al., LLNL/UC AMS facility and research program: Nuclear instruments and methods, *Phys. Res.*, 269–272, 1990.

Deng, Q., et al., Variations in the geometry and amount of slip on the Haiyuan (Nanxihaushan) fault zone, China, and the surface rupture of the 1920 Haiyuan earthquake, in *Earthquake Source Mechanics, Geophys. Monogr. Ser.*, vol. 37, edited by S. Das et al., pp. 169–182, AGU, Washington, D. C., 1986.

Derbyshire, E., Y. Shi, J. Li, B. Zheng, S. Li, and J. Wang, Quaternary glaciation of Tibet: The geological evidence, *Quat. Sci. Rev.*, 10, 485–510, 1991.

Fluteau, F., G. Ramstein, and J. Besse, Simulating the evolution of the Asian and African monsoons during the past 30 Myr using an atmospheric general circulation model, *J. Geophys. Res.*, 104, 11,995–12,018, 1999.

Gansu Geological Bureau, Geological map of Gansu, scale 1:1,000,000, Geol. Press, Beijing, 1975a.

Gansu Geological Bureau, Geological map of Gansu, scale 1:200,000, Geol. Press, Beijing, 1975b.

Gaudemer, Y., P. Tapponnier, B. Meyer, G. Peltzer, S. Guo, Z. Chen, H. Dai, and I. Cifuentes, Partitioning of crustal slip between linked active faults in the eastern Qilian Shan, and evidence for a major seismic gap, the "Tianzhu gap", on the western Haiyuan fault, Gansu (China), *Geophys. J. Int.*, 120, 599–645, 1995.

Gosse, J., and F. M. Phillips, Terrestrial in situ cosmogenic nuclides: Theory and application, *Quat. Sci. Rev.*, 20, 1475–1560, 2001.

Gu, G., T. Lin, and Z. Shi, *Catalogue of Chinese Earthquakes (1831 BC–1969 AD)*, Science Press, Beijing, 1989.

Kohl, C. P., and K. Nishiizumi, Chemical isolation of quartz for measurement of in situ produced cosmogenic nuclides, *Geochim. Cosmochim. Acta*, 56, 3583–3588, 1992.

Lal, D., Cosmic ray labelling of erosion surfaces: In situ nuclide production rates and erosion models, *Earth Planet. Sci. Lett.*, 104, 424–439, 1991.

Lasserre, C., et al., Postglacial left slip-rate and past occurrence of $M \geq 8$ earthquakes on the western Haiyuan fault, Gansu, China, *J. Geophys. Res.*, 104, 17,633–17,651, 1999.

Lehmkuhl, F., L. A. Owen, and E. Derbyshire, Late Quaternary glacial history of northeast Tibet, in *Mountain Glaciation, Quat. Proc.*, no. 6, edited by L. A. Owen, pp. 121–142, John Wiley, New York, 1998.

Liu, K. B., Z. Yao, and L. G. Thompson, A pollen record of Holocene climatic changes from the Dunde ice cap, Qinghai-Tibetan Plateau, *Geology*, 26, 135–138, 1998.

Mériaux, A.-S., Détermination par datation cosmogénique des variations de la vitesse de glissement sur la faille de l'Altyn Tagh depuis 100 ka, Ph.D. thesis, Univ. Paris VII, Paris, 2002.

Mériaux, A.-S., P. Tapponnier, F. Ryerson, J. Van der Woerd, G. King, R. Meyer, B. Finkel, and M. Caffee, Application of cosmogenic [10]Be and [26]Al dating to neotectonics of the Altyn Tagh fault in central Asia (Gansu, China), *Eos Trans. AGU, 78*(46), Fall Meet. Suppl., 1997.

Mériaux, A.-S., F. Ryerson, P. Tapponnier, J. Van der Woerd, C. Lasserre, and X. Xiwei, Large-scale strain patterns, great earthquakes, and late Pleistocene slip rate along the Altyn Tagh fault (China), *Eos Trans. AGU, 79*(45), Fall Meet. Suppl., 1998.

Meyer, B., Mécanismes des grands tremblements de terre et du raccourcissement crustal oblique au bord nord-est du Tibet, Ph.D. thesis, Univ. de Paris VII, Paris, 1991.

Meyer, B., P. Tapponnier, L. Bourjot, F. Métivier, Y. Gaudemer, G. Peltzer, S. Guo, and Z. Chen, Crustal thickening in Gansu-Qinghai, lithospheric mantle subduction, and oblique, strike-slip controlled growth of the Tibet Plateau, *Geophys. J. Int., 135*, 1–47, 1998.

Molnar, P., and P. Tapponnier, Active tectonics of Tibet, *J. Geophys. Res., 83*, 5361–5375, 1978.

Nishiizumi, K., E. L. Winterer, C. P. Kohl, J. Klein, R. Middleton, D. Lal, and J. R. Arnold, Cosmic ray production rates of [10]*Be* and [26]*Al* in quartz from glacially polished rocks, *J. Geophys. Res., 94*, 17,907–17,915, 1989.

Owen, L. A., R. C. Finkel, M. W. Caffee, and L. Gualtieri, Timing of multiple glaciations in the late Quaternary in the Hunza valley, Karakoram Mountains, northern Pakistan: Constrained by cosmogenic radionuclide dating of moraines, *Geol. Soc. Am. Bull., 114*, 593–604, 2002.

Peltzer, G., and F. Saucier, Present-day kinematics of Asia derived from geological fault rates, *J. Geophys. Res., 101*, 27,943–27,956, 1996.

Ramstein, G., F. Fluteau, J. Besse, and S. Joussaume, Effect of orogeny, plate motion and land-sea distribution on Eurasian climate change over the past 30 million years, *Nature, 386*, 788–795, 1997.

Shi, Y., B. Ren, J. Wang, and E. Derbyshire, Quaternary glaciations in China, *Quat. Sci. Rev., 5*, 503–507, 1986.

Stone, J. O., Air pressure and cosmogenic isotope production, *J. Geophys. Res., 105*, 23,753–23,759, 2000.

Tapponnier, P., and P. Molnar, Active faulting and tectonics in China, *J. Geophys. Res., 82*, 2905–2930, 1977.

Thompson, L. G., et al., Tropical climate instability: the Last Glacial Cycle from a Qinghai-Tibetan ice core, *Science, 276*, 1821–1825, 1997.

Van der Woerd, J., F. J. Ryerson, P. Tapponnier, Y. Gaudemer, R. Finkel, A. S. Mériaux, M. Caffee, G. Zhao, and Q. He, Holocene left-slip rate determined by cosmogenic surface dating on the Xidatan segment of the Kunlun fault (Qinghai, China), *Geology, 26*, 695–698, 1998.

Van der Woerd, J., et al., Uniform slip-rate along the Kunlun fault: Implications for seismic behaviour and large-scale tectonics, *Geophys. Res. Lett., 27*, 2353–2356, 2000.

Van der Woerd, J., et al., Uniform Post-Glacial slip-rate along the central 600 km of the Kunlun fault (Tibet), from [26]Al,[10]Be and ^{14}C dating of river offsets, and climatic origin of the regional morphology, *Geophys. J. Int., 148*, 356–388, 2002.

Weldon, R. J., and K. E. Sieh, Holocene rate of slip and tentative recurrence interval for large earthquakes on the San Andreas fault, Cajon Pass, southern California, *Geol. Soc. Am. Bull, 96*, 793–812, 1985.

Zhang, P., P. Molnar, B. C. Burchfiel, L. H. Royden, Y. Wang, Q. Deng, F. Song, W. Zhang, and D. Jiao, Bounds on the Holocene slip rate of the Haiyuan fault, north-central China, *Quat. Res., 30*, 151–164, 1988a.

Zhang, P., P. Molnar, W. Zhang, Q. Deng, Y. Wang, B. C. Burchfiel, F. Song, L. H. Royden, and D. Jiao, Bounds on the average recurrence interval of major earthquakes along the Haiyuan fault in north-central China, *Seismol. Res. Lett., 59*, 81–89, 1988b.

Zhang, W., D. Jiao, P. Zhang, P. Molnar, B. C. Burchfiel, Q. Deng, Y. Wang, and F. Song, Displacement along the Haiyuan fault associated with the great 1920 Haiyuan, China, earthquake, *Bull. Seismol. Soc. Am., 77*, 117–131, 1987.

Y. Gaudemer, A.-S. Mériaux, and P. Tapponnier, Institut de Physique du Globe de Paris, CNRS UMR 7578, 4, place Jussieu, 75252 Paris Cédex 05, France. (gaudemer@ipgp.jussieu.fr; ameriaux@ipgp.jussieu.fr; tappon@ipgp.jussieu.fr)

D. Yuan, Lanzhou Institute of Seismology, China Seismological Bureau, 410, Donggangxilu Avenue, Lanzhou, Gansu 730000, China.

C. Lasserre, Department of Earth and Space Sciences, University of California, Los Angeles, 595 Charles Young Drive East, 3806 Geology Bldg./Box 951567, Los Angeles, CA 90095-1567, USA. (cecile@ess.ucla.edu)

F. J. Ryerson, Lawrence Livermore National Laboratory, P.O. Box 808, L202, Livermore, CA 94551, USA. (ryerson@s91.es.llnl.gov)

J. Van der Woerd, Institut de Physique du Globe de Strasbourg, CNRS UML 7516, 5 rue René Descartes, F-67084 Strasbourg Cedex, France. (Jerome.Vanderwoerd@eost.u-strasbg.fr)